Supporting Information

Mimosa-inspired photothermal-responsive multifunctional hydrogel for solar-drive efficient water purification

Jiangyang Mei,[ab] Yong Jin,[ab] Long Bai,[ab] Xiang Shang,[ab] Wenhua Zeng[ab]*

[a] National Engineering Research Center of Clean Technology in Leather Industry, Sichuan University, Chengdu 610065, PR China

[b] Key Laboratory of Leather Chemistry and Engineering of Ministry of Education, Sichuan University, Chengdu 610065, PR China

* Corresponding Author: Yong Jin, E-mail: jinyong@cioc.ac.cn.

This material includes:

1. Experimental section

2. Supporting Figures

Fig. S1 Preparation of hydrogels.

Fig. S2 Compressive stress-strain curves of hydrogels of PNIPAm/CMC/CMCNT with different CMCNT contents.

Fig. S3 Compressive stress-strain curves of hydrogels of PNIPAm/CMC/CMCNT with different CMC contents.

Fig. S4 Digital photographs of the hydrogels with different components after water swelling.

Fig. S5 Shapes of the hydrogels with different components before and after compression treatment.

Fig. S6 Tension stress-strain of hydrogels with different components under 0, 30 and 150wt% water absorption conditions (a:PNIPAm/CMC/CMCNT hydrogel, b:PNIPAm/CMC hydrogel, c:PNIPAm/CMCNT hydrogel, d:PNIPAm hydrogel).

Fig. S7 Young's modulus of hydrogels with different components under 0, 30 and 150wt% water absorption conditions.

Fig. S8 Optical images showing the dynamic wetting behaviors of a water droplet atop PNIPAm /CMC/CMCNT hydrogel with different CMC and CMCNT contents at room temperature.

Fig. S9 Schematic diagram of the phase transition response mechanism of PNIPAm at

the temperature around its LCST.

Fig. S10 Tatent enthalpy of phase transformation for PNIPAm/CMC/CMCNT hydrogel.

Fig. S11 Water release efficiency of the PNIPAm/CMC/CMCNT hydrogel under different sun irradiation.

Fig. S12 Water release efficiency of PNIPAm/CMC/CMCNT hydrogel with different cycle times under one sun irradiation.

Fig. S13 UV-vis spectrum of different dyes removal by PNIPAm/CMC/CMCNT hydrogel: (a) Methylene blue solution, (b) Eosin Y solution, (c) Bromophenol blue solution, and (d) rhodamine 6G solution.

Fig. S14 Changes of ion concentration in wastewater before and after purification of PNIPAm/CMC/CMCNT hydrogel.

Fig. S15 Changes of Na^+ concentration in wastewater before and after purification of hydrogels with different components.

Fig. S16 Changes of Mg^{2+} concentration in wastewater before and after purification of hydrogels with different components.

Fig. S17 Antibacterial properties of the hydrogels

Fig. S18 Photographs of the PNIPAm/CMC/CMCNT hydrogel floating atop Dong Lake.

Fig. S19 Surface temperature change of PNIPAm/CMC/CMCNT hydrogel under natural sunlight.

3. Supporting Movie

Movie S1 Cycle times fatigue test for PNIPAm/CMC/CMCNT hydrogel.

1. Materials and methods

***Materials*:** N,N'-Methylenebisacrylamide (Bis, 99.0%) was bought from Aladdin. N-Isopropylacrylamide (NIPAm, 98.0%) and carboxymethyl chitosan(CMC) were purchased from Energy Chemical. Carboxylic multi-walled carbon nanotubes (CMCNT, 98.0%) were taken from XFNANO. Ammonium persulfate (APS) and N,N,N',N'-tetramethyl-ethylenediamine (TEMED) were obtained from Sigma-Aldrich.

***Preparation of the PNIPAm/CMC/CMCNT hydrogel*:** The PNIPAm/CMC/CMCNT hydrogel was prepared by a simple two-step polymerization process in an aqueous solution without using an emulsifier. First, 150 mg of NIPAm, 8 mg of APS, and 8 mg of Bis were added to 6 mL of aqueous solution containing 30 mg of CMC. To remove oxygen, nitrogen was bubbled through the mixed solution for 30 minutes and then held at 34 ℃ for 15 minutes to form the NIPAm pre-polymerization solution. Then, 0.85 g of NIPAm was added at 100 rpm until complete dissolution. The mixed solution was held at 8 ℃ for 15 minutes and 300 μL (0.2 $g \cdot mL^{-1}$) CMCNT was added. 40 μL of TEMD was in addition to the system to provide free radicals to accelerate the reaction, and PNIPAm/CMC/CMCNT hydrogel was formed 30 minutes later. Other control samples were prepared, including PNIPAm hydrogel, PNIPAm/CMC hydrogel, and PNIPAm-CMCNT hydrogel.

***Characterization of hydrogels*:** All assays in this experiment occurred during the winter months. Dynamic wetting was observed on the water contact angle (HARKE,

SPCAX1). A Fourier infrared spectrometer was employed to obtain Fourier transform infrared spectroscopy (IS10, PerkinElmer). Digital photographs of hydrogels at different temperatures were taken by a camera with an infrared thermal imager (E5 Systems, FLIR). The 2 mm thick hydrogels were attached to the inner wall to measure the transmittance of materials by an ultraviolet-visible near infrared spectrophotometer (U-3900, PerkinElmer). The LCST of hydrogels was measured by a differential scanning calorimeter(DSC204F01, Netzsch). A scanning electron microscope (Helios G4 UC, Thermo Fisher SCIENTIFIC) was used to observe the microstructure of a series of complex hydrogels. Dynamic mechanical analysis was determined using a rotational rheometer (MCR302, Anton Paar) with a 25 mm diameter platform, which included dynamic frequency scanning and temperature sweep. The temperature sweep was measured under 1% strain and 1 Hz frequency at temperatures of 25 to 50 ℃ and the dynamic frequency scanning was obtained under 1% strain and 25 ℃ at a frequency of 0.1 to 100 Hz.

***Mechanical performance experiments*:** The mechanical properties of materials were tested by a universal material testing machine (Gotech, AI-7000SN). Compression property was recorded at room temperature, whose strain rate was 30 $mm \cdot min^{-1}$. The initial standard distance between the two compression clamps was set to 25 mm. The cylindrical sample with a diameter of 20 mm and a height of 25 mm was used for compression tests. Compression test conditions were crosshatched speed 10 $mm \cdot min^{-1}$, initial distance 25 mm. Meanwhile, to measure the recovery performance of cyclic compression, the sample was compressed to a predetermined

80% strain and then unloaded at the same speed. Five consecutive load-unload cycles were conducted on the sample under the same compression mode.

***Photothermal conversion efficiency and surface temperature test of PNIPAm/CMC/CMCNT hydrogel*:** The mass loss and surface temperature of the PNIPAm/CMC/CMCNT hydrogel were measured by a photochemical reactor (CEL-HXF300, CEAULIGHT) with a xenon arc lamp emitting simulated radiation intensity of 1 $kW \cdot m^{-2}$ (300 W).

The photothermal conversion efficiency (η) can be calculated by the following equation:[1]

$$\eta = \frac{W\Delta H_{equ}}{I} \times 100\% \qquad (1)$$

η: photothermal conversion efficiency of the hydrogel;

W: water collection rate of the hydrogel, $kg \cdot m^{-2} \cdot h^{-1}$;

ΔH_{equ}: total latent enthalpy of phase transformation and water evaporation for the hydrogel, $J \cdot kg^{-1}$;

I: nominal direct solar illumination (1 $kW \cdot m^{-2}$);

***Removal rate of the dye*:**

$$R = \frac{S_0}{S} \times 100\% \qquad (2)$$

R: dye removal rate by hydrogels;

S_0: the area of the UV-Vis spectrum of water collected by hydrogel treatment after;

S: the area of the UV-Vis spectrum of the solution by water mixed with dyes.

Removal rate of metal ions:[31]

$$Q_0 = \frac{C_0(V_0 - V_1)}{M} \qquad (3)$$

$$Q_e = \frac{C_e V_2}{M} \qquad (4)$$

Q_0: adsorption capacity of Cr^{3+}/Cd^{2+} after hydrogel treatment for 2 h, ppm;

C_0: initial concentration of Cr^{3+}/Cd^{2+} in a sewage model, $mg \cdot L^{-1}$;

V_0: initial volume of Cr^{3+}/Cd^{2+} in a sewage model, L;

V_1: residual volume of Cr^{3+}/Cd^{2+} in sewage model after 2h adsorption by hydrogel, L;

M: quality of the hydrogel, kg;

C_e: concentration of Cr^{3+}/Cd^{2+} in the clear water, which is released from the PNIPAm/CMC/CMCNT hydrogel, $mg \cdot L^{-1}$;

V_2: volume of the clear water, which is released by the PNIPAm/CMC/CMCNT hydrogel, L;

Q_e: residual capacity of Cr^{3+}/Cd^{2+} after the PNIPAm/CMC/CMCNT hydrogel, ppm.

Water collection and practical application test: A photochemical reactor with a xenon arc lamp emitting a simulated radiation intensity of 1 $kW \cdot m^{-2}$ (300 W, one sun) was used to test the water-holding capacity and water purification of PNIPAm/CMC/CMCNT hydrogel. To measure the water purification capability of the hydrogels, the dyes, microbes, oil, and heavy metals were mixed with water as sample contaminants respectively. Meanwhile, practical decontamination applications were tested by a water purification system fabricated from PNIPAm/CMC/CMCNT

hydrogel with 9 cm×9.0 cm×1.0 cm square shape floating atop Dong Lake (Chengdu, China) to absorb water for 2 h, and then place the PNIPAm/CMC/CMCNT hydrogel in a transparent closed system with multi void plate spacing to collect purified water under natural light.

Bactericidal function test: Gram-negative bacteria E. coli and Gram-positive bacteria S. aureus were used to evaluate the antimicrobial activity of the hydrogels with the spread plate count method. 10 mg of each sample film was added into 20 mL of bacteria solution with a concentration of ~10^7 colony-forming units per mL (CFU·mL^{-1}). After shaking for 2 h at 37 ℃ with continuous oscillation, the bacterial solution was gradient diluted and instantly coated on the nutrient agar medium plates. All the coated plates were incubated at 37 ℃ in a constant temperature incubator for 24 h.

$$\mathrm{P} = \frac{A - B}{A} \times 100\% \qquad (5)$$

P: bactericidal rate of hydrogels;

A: bacteria number of negative control;

B: bacteria number of sample hydrogels.

2. Supplementary Figures

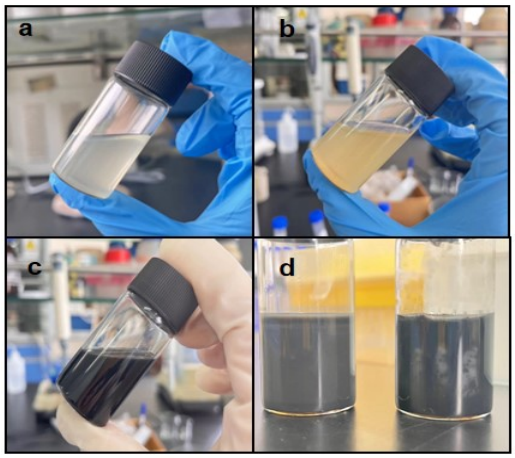

Fig. S1 Preparation of hydrogels. (a) NIPAm pre-polymerization solution. (b) PNIPAm/CMC prepolymerization solution. (c) PNIPAm/CMC/CMCNT hydrogel prepolymerization solution. (d) PNIPAm/CMC/CMCNT hydrogel (left) and PNIPAm/CMC/CWCNTs hydrogel (right) with the addition of CMCNT first.

As shown in Fig. S1, the PNIPAm/CMC/CMCNT hydrogel was prepared by a one-pot method, where the order of addition of CMCNT was particularly important. For example, the aggregation of CMCNT was found in the hydrogel prepared with CMCNT added before the formation of the PNIPAm/CMC pre-polymerization solution (Fig. S1d-right). On the contrary, a uniform PNIPAm/CMC/CMCNT hydrogel could be obtained when the CMCNT was added after the formation of the PNIPAm/CMC pre-polymerization solution, as shown in Fig. S1d-left, which also confirmed the successful and well-controlled deposition of the CMCNT.

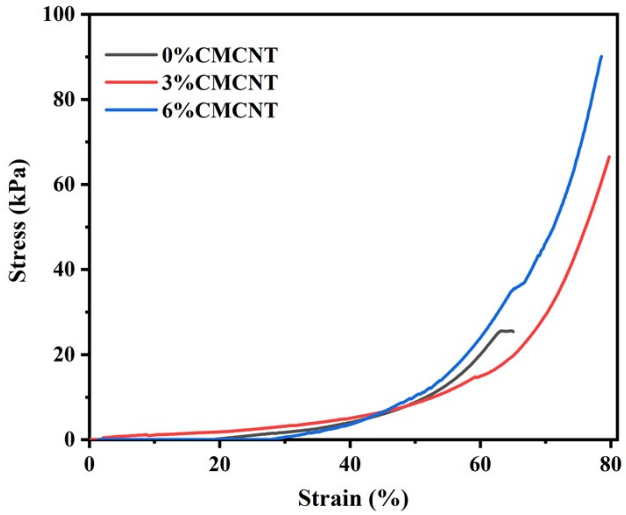

Fig. S2 Compressive stress-strain curves of the PNIPAm/CMC/CMCNT hydrogel with different CMCNT contents.

The content of different components is essential for the mechanical properties of the hydrogels. As shown in Fig. S2, the compressive stress of PNIPAm/CMC/CMCNT hydrogel increases as the CMCNT content increases from 0% to 6%. The aggregation of CMCNT in the hydrogel is observed when the CMCNT content is above 6%, as shown in Fig. S2.

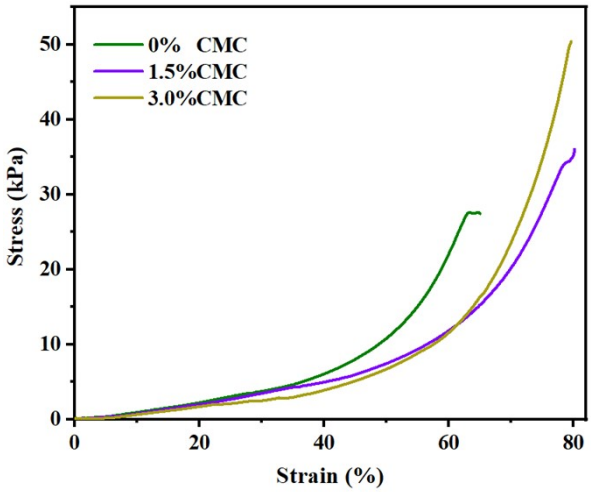

Fig. S3 Compressive stress-strain curves of the PNIPAm/CMC/CMCNT hydrogel with different CMC contents.

The compressive stress of the PNIPAm/CMC/CMCNT hydrogel increases with increasing the CMC content from 0% to 3% (Fig. S3). In contrast, the PNIPAm/CMC/CMCNT solution is not sufficiently mixed to form a hydrogel, and aggregation occurs at the CMC content above 3%.

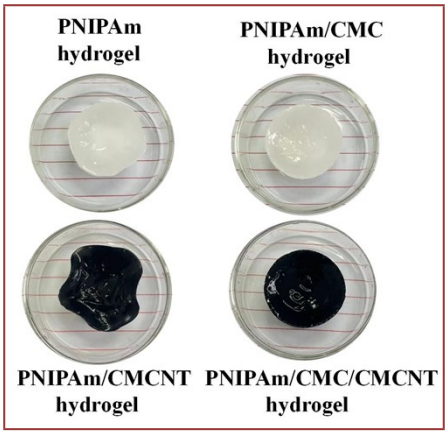

Fig. S4 Digital photographs of the hydrogels with different components.

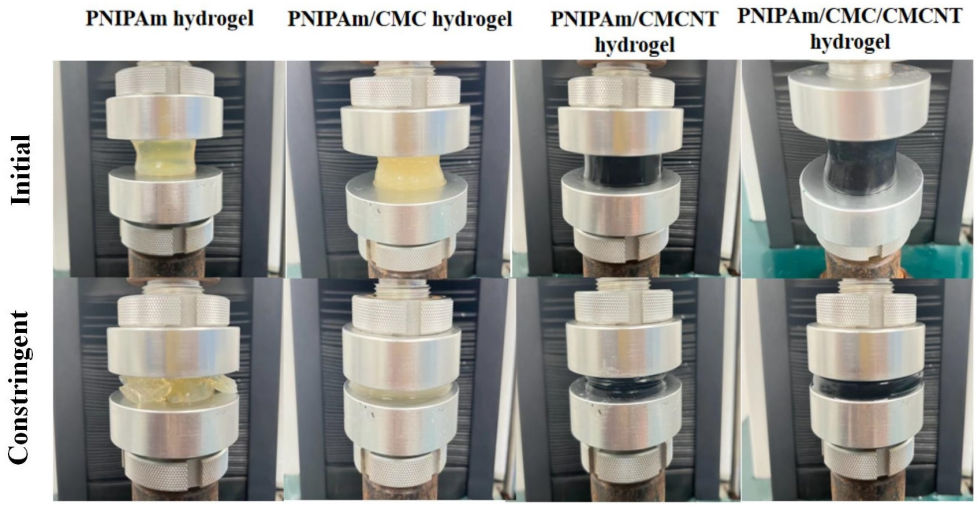

Fig. S5 Shapes of the hydrogels with different components before and after compression treatment.

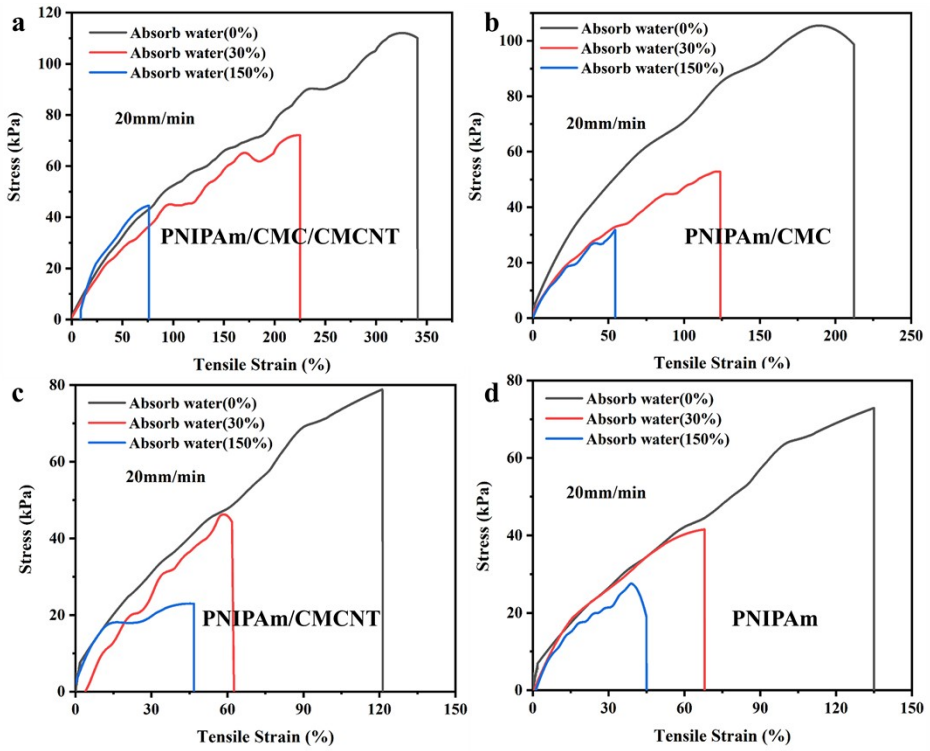

Fig. S6 Tension stress-strain of hydrogels with different components under 0, 30 and 150wt% water absorption conditions (a:PNIPAm/CMC/CMCNT hydrogel, b:PNIPAm/CMC hydrogel, c:PNIPAm/CMCNT hydrogel, d:PNIPAm hydrogel).

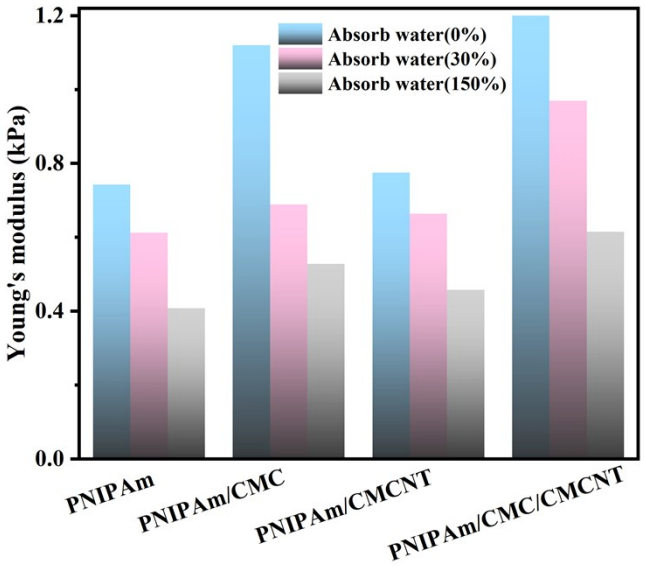

Fig. S7 Young's modulus of hydrogels with different components under 0, 30 and 150wt% water absorption conditions.

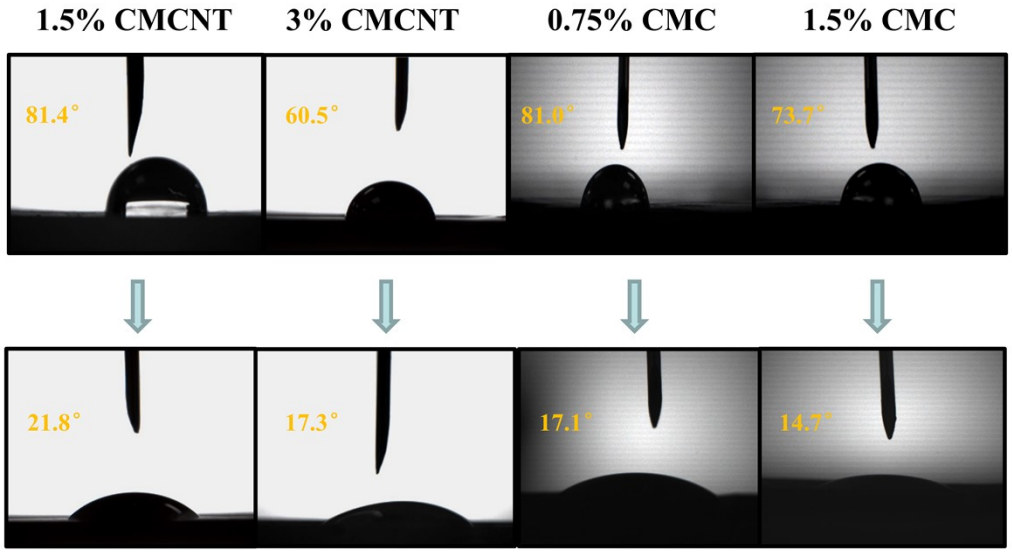

Fig. S8 Optical images showing the dynamic wetting behaviors of a water droplet atop PNIPAm /CMC/CMCNT hydrogel with different CMC and CMCNT contents at room temperature.

As shown in Fig. S6, the water contact angle (WCA) of PNIPAm/CMC/CMCNT hydrogel with different CMC and CMCNT decreases with increasing the CMCNT and CMC contents. When 3% CMC is added to form PNIPAm/CMC/CMCNT hydrogel, the WCA value of the hydrogel decreases from 21.8° to 17.3° with the addition of CMCNT increases from 1.5% to 3%. Meanwhile, when the amount of CMCNT in PNIPAm/CMC/CMCNT hydrogel is 6%, the WCA of the hydrogel reduces from 17.1° to 14.7° with the CMC contents increasing from 0.75% to 1.5%.

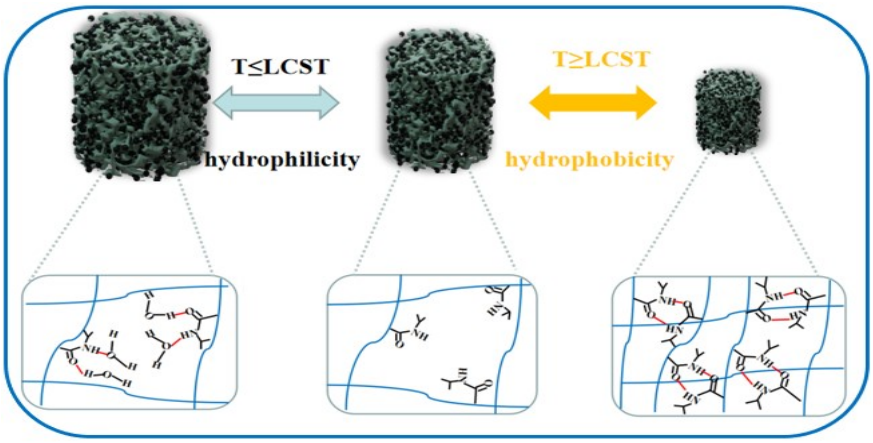

Fig. S9 Schematic diagram of the phase transition response mechanism of PNIPAm at the temperature around its LCST.

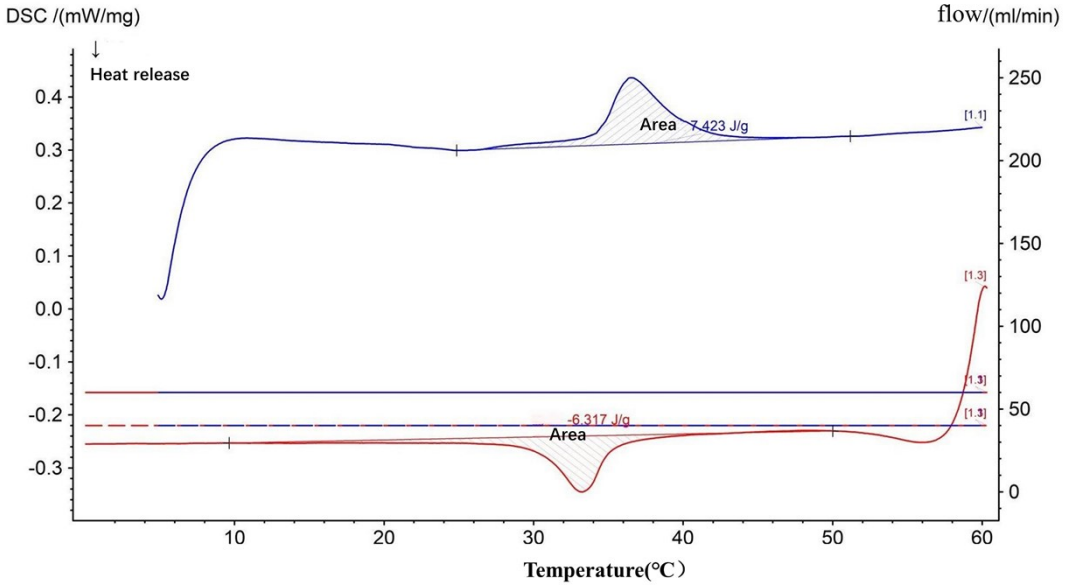

Fig. S10 Tatent enthalpy of phase transformation for PNIPAm/CMC/CMCNT hydrogel.

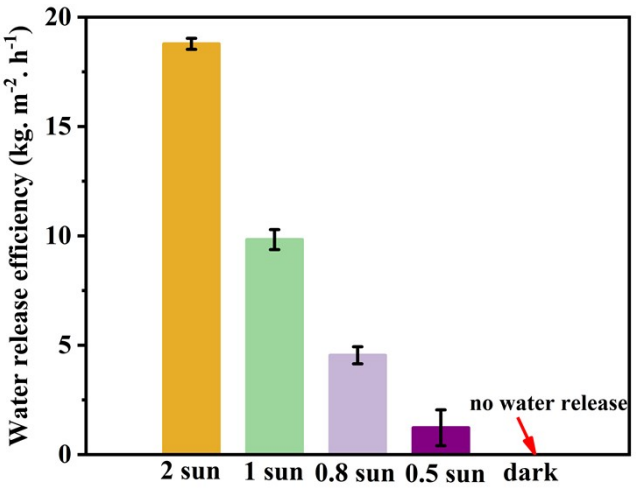

Fig. S11 Water release efficiency of the PNIPAm/CMC/CMCNT hydrogel under different sun irradiation.

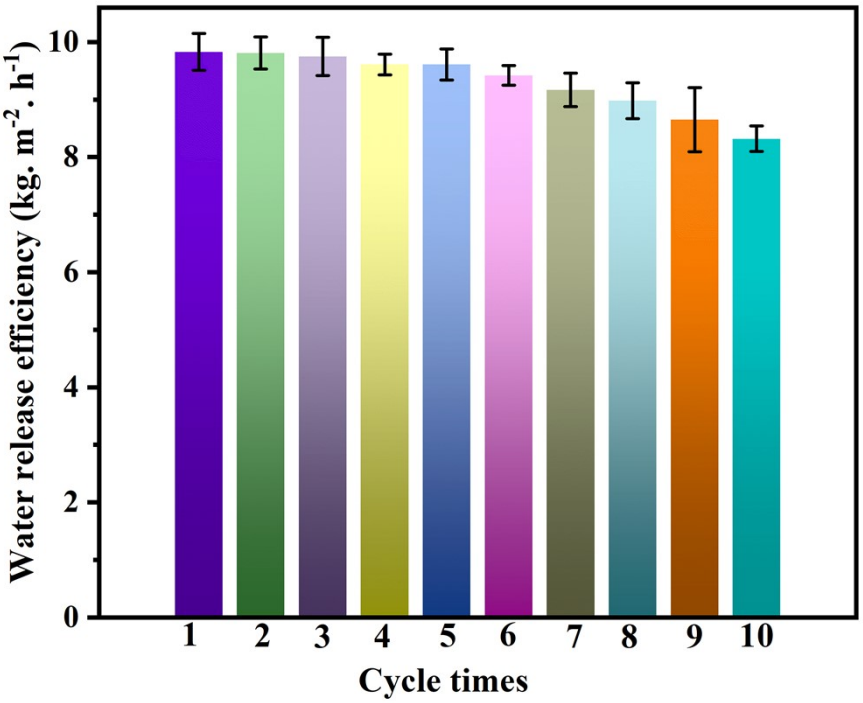

Fig. S12 Water release efficiency of the PNIPAm/CMC/CMCNT hydrogel with different cycle times under one sun irradiation.

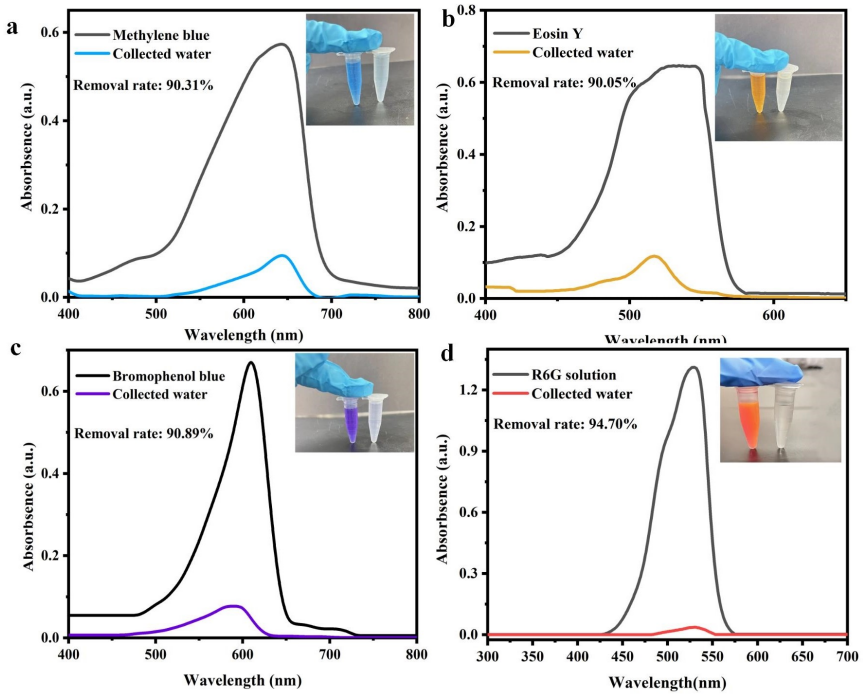

Fig. S13 UV-vis spectrum of dyes removal by the PNIPAm/CMC/CMCNT hydrogel: (a) Methylene blue solution, (b) Eosin Y solution, (c) Bromophenol blue solution and (d) rhodamine 6G solution.

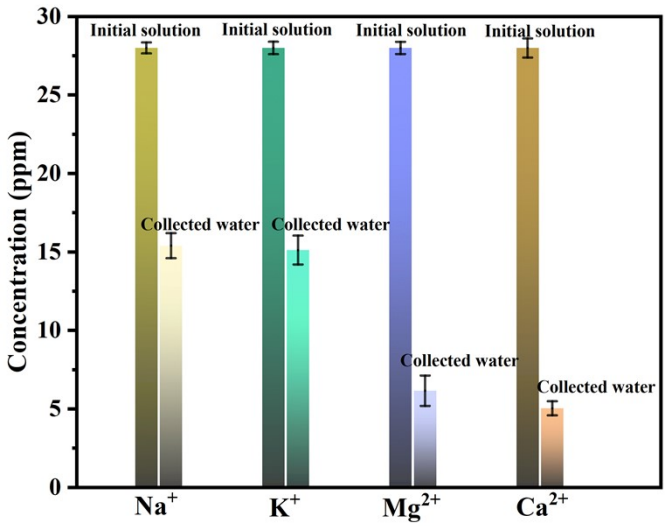

Fig. S14 Changes of ion concentration in wastewater before and after purification of PNIPAm/CMC/CMCNT hydrogel.

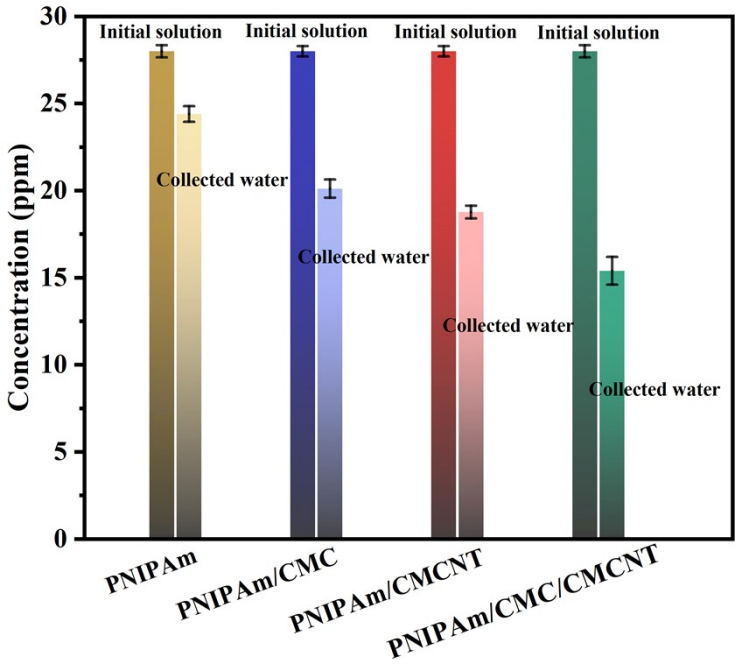

Fig. S15 Changes of Na^+ concentration in wastewater before and after purification of hydrogels with different components.

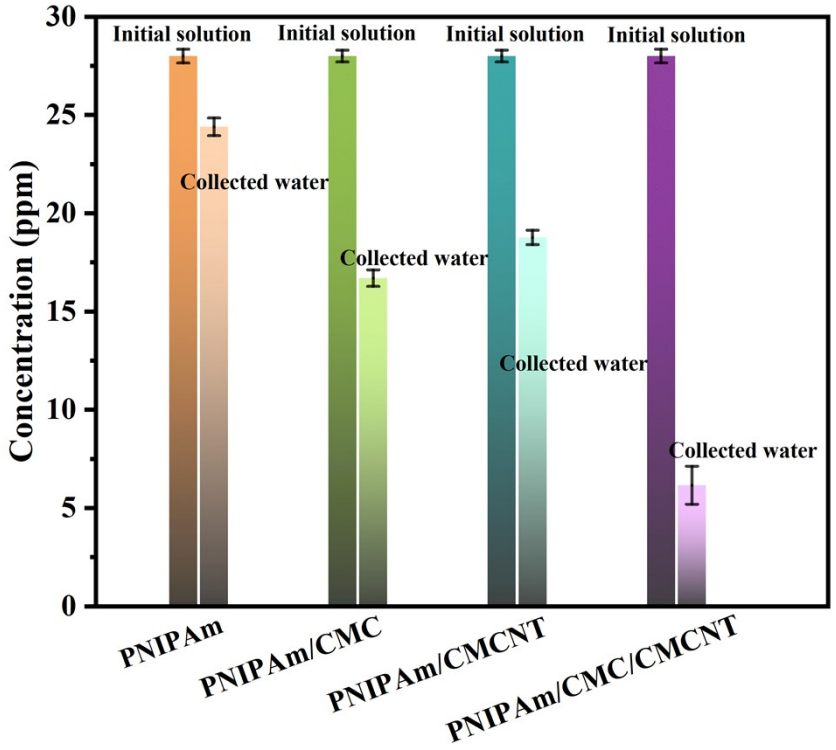

Fig. S16 Changes of Mg^{2+} concentration in wastewater before and after purification of hydrogels with different components.

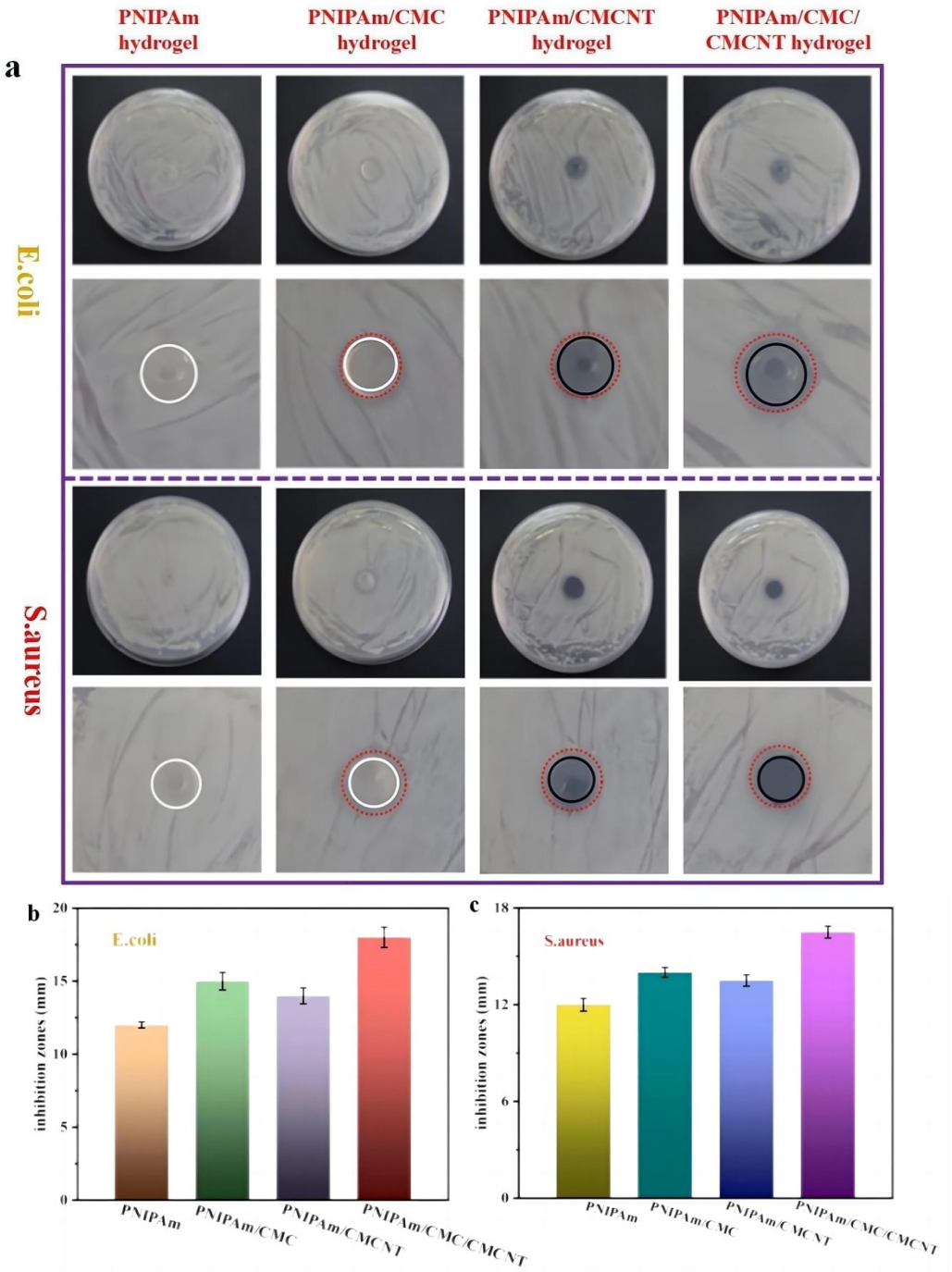

Fig. S17 (a) Antibacterial properties of the hydrogels against E.coli and S. aureus. Diameter of inhibition zones against E.coli (b) and S.aureus (c) by PNIPAm-based hydrogels.

As illustrated in Fig. S13, the antimicrobial zones of the hydrogel containing CMC or CMCNT against E. coli and S. aureus were different, and no inhibitory

regions were observed in the PNIPAm membrane, while PNIPAm/CMC, PNIPAm/CMCNT and PNIPAm/CMC/CMCNT membranes showed significant inhibitory zones on both E. coli and S. aureus agar plates. Specifically, the diameter of the E. coli inhibition zone on the surfaces of PNIPAm, PNIPAm/CMC, PNIPAm/CMCNT, and PNIPAm/CMC/CMCNT hydrogels were 12 mm, 15 mm, 14 mm, and 18 mm respectively, while the diameter of the S. aureus inhibition zone was 12 mm, 14 mm, 13 mm, and 16.5 mm respectively, as displayed in Fig S13(b,c). Evidently, the PNIPAm/CMC/CMCNT hydrogel exhibited excellent bactericidal activity and resulted in the largest bacteriostatic zones.

Fig. S18 Photographs of the PNIPAm/CMC/CMCNT hydrogel floating atop Dong Lake.

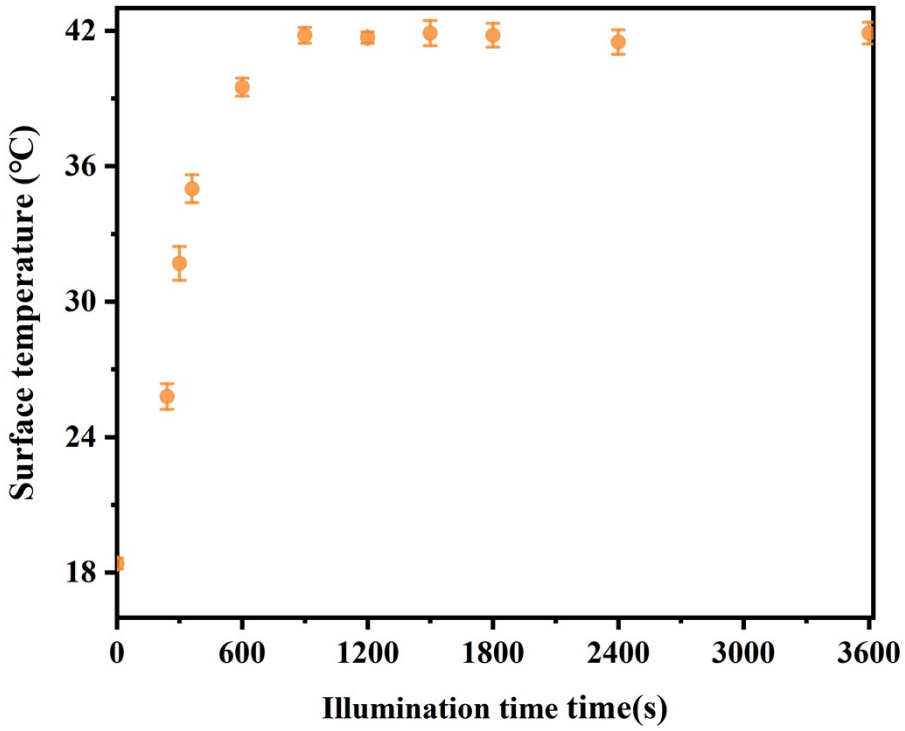

Fig. S19 Surface temperature change of the PNIPAm/CMC/CMCNT hydrogel under natural sunlight.

3. Supporting Movie

Supporting Movie S1: See attachment MovieS1

References:

[1] S. A. Cheng, Z. Yu, Z. F. Lin, L. X. Li, Y. H. Li, Z. Z. Mao, Chem. Eng. J., 2020, 401, 126108.